Resonantly Enhanced Multiphoton Ionization and Zero Kinetic Energy Photoelectron Spectroscopy of Benzo[g,h,i]perylene

ARTICLE *in* THE JOURNAL OF PHYSICAL CHEMISTRY A · FEBRUARY 2012

Impact Factor: 2.69 · DOI: 10.1021/jp2109576 · Source: PubMed

3 AUTHORS, INCLUDING:

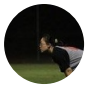

Jie Zhang
Oregon State University
18 PUBLICATIONS **130** CITATIONS

THE JOURNAL OF PHYSICAL CHEMISTRY A

Article

pubs.acs.org/JPCA

Resonantly Enhanced Multiphoton Ionization and Zero Kinetic Energy Photoelectron Spectroscopy of Benzo[*g,h,i*]perylene

Jie Zhang, Colin Harthcock, and Wei Kong*

Department of Chemistry, Oregon State University, Corvallis, Oregon 97331-4003, United States

ABSTRACT: We report zero kinetic energy (ZEKE) photoelectron spectroscopy of benzo[*g,h,i*]perylene (B*ghi*P) via resonantly enhanced multiphoton ionization (REMPI). Our analysis concentrates on the vibrational modes of both the first electronically excited state and the ground cationic state. Extensive vibronic coupling due to a nearby electronically excited state manifests through strong Franck−Condon (FC) forbidden bands, which are stronger than even the FC allowed bands in the REMPI spectrum. Theoretical calculations using Gaussian are problematic in identifying the electronic configurations of the excited electronic states and predicting the transition energies. However, by setting the keyword for the second excited electronic state, both density functional theory and configuration interaction methods can reproduce the observed spectrum qualitatively. The general agreement significantly helps with the vibrational assignment. The ZEKE spectra demonstrate propensity in preserving the vibrational excitation of the intermediate electronic state. In addition, almost all ZEKE spectra exhibit a similar vibrational distribution, and the distribution can be reproduced by an FC calculation from the vibronic origin of the first excited electronic state to the cationic state using Gaussian 09. These results suggest a remarkable structural stability of B*ghi*P in accommodating the additional charge. All observed vibrational bands of the cation are IR active, establishing the role of ZEKE spectroscopy in mapping out far-infrared bands for astrophysical applications.

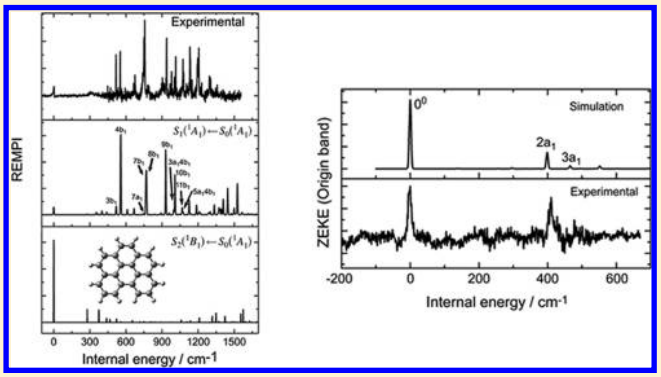

INTRODUCTION

Polycyclic aromatic hydrocarbons (PAH) are a group of compounds distributed in the environment, in comet tails, and perhaps in outer space.[1] Environmental PAHs are formed during incomplete combustion of organic substances and are related to environmental toxicity and carcinogenicity.[2,3] In astrophysics, PAHs have been observed in a wide range of galactic and extragalactic regions, and they have been further suggested to be related to the origin of life via the formation of primitive organic molecules including amino acids in the pre-DNA world.[4−7]

Both neutral and ionic PAHs are considered promising candidates for the interstellar absorption and emission bands,[8−15] hence spectroscopic investigations of PAHs and their cations in both infrared and ultraviolet/visible regions have been explored using photoionization spectroscopy,[16] cavity ringdown,[17] and infrared absorption and emission spectroscopy.[18] The far-infrared (FIR) region is occupied by skeletal modes of the molecular frame, and it is considered the "finger-print region" for spectroscopic identification of astrophysical PAHs.[12,19,20] However, the FIR region was once considered "no man's land" because of the low sensitivity of available detectors and the low intensity of available light sources. Moreover, laboratory experiments of ions are further challenged by the achievable low ion densities.

The technique of zero kinetic energy (ZEKE) photoelectron spectroscopy offers an indirect solution to these challenges in laboratory astrophysics in the FIR.[21−23] ZEKE is known for its high resolution (on the order of ∼100 kHz) of cation rovibrational spectroscopy.[24] The high Rydberg states in ZEKE are longer lived when they are associated with lower vibronic states of the cation, which makes it particularly suitable for studies of low frequency vibrational modes. By detecting electrons from pulsed field ionization in ZEKE spectroscopy via multiphoton excitation, both the light source and the detector problems in typical FIR and submillimeter wave experiments can be avoided. Controlled by the Franck−Condon (FC) principle, the vibrational modes from ZEKE are different from those governed by single photon vibrational transitions. However, the IR forbidden modes from ZEKE are useful for frequency calibration and for determination of scaling factors from theoretical calculations. Moreover, to model the energy balance in the interstellar medium,[8,25−27] both IR allowed and forbidden modes are necessary.

In this report, we investigate the electronic and vibrational spectroscopy of benzo[*g,h,i*]perylene (B*ghi*P), also known as 1,12-benzoperylene, as shown in the inset of Figure 1. The first two excited electronic states of this peri-condensed PAH have been widely studied both experimentally and theoretically in the gas phase and in the solution phase.[28−33] Helium droplet

Received: November 14, 2011
Revised: January 9, 2012
Published: January 18, 2012

dx.doi.org/10.1021/jp2109576 | *J. Phys. Chem. A* 2012, 116, 1551−1557

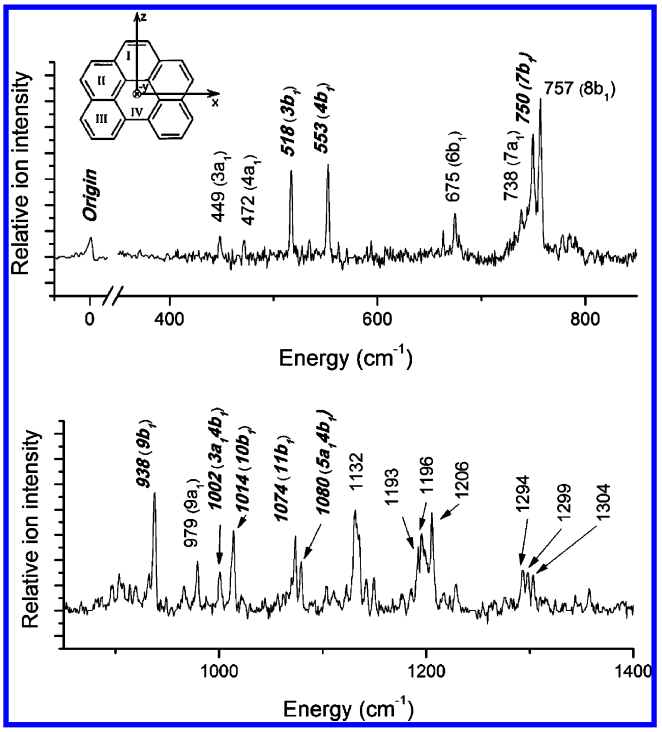

Figure 1. The (1 + 1′) REMPI spectrum of jet-cooled B*ghi*P in the S_1 electronic state. The spectrum is shifted by 25 027 cm^{-1} (the origin of the $S_1 \leftarrow S_0$ transition) to emphasize the frequencies of the different vibrational levels of the S_1 state. The assignments to these transitions are listed in Table 1. Both the vibrational energies in cm^{-1} and symmetry assignments are labeled in the figure. Bold and italicized labels represent intermediate states from which ZEKE spectra were collected. The inset shows the molecular structure and the orientation of molecular axes.

studies have explored the vibrational spectroscopy of the S_1 state up to 3530 cm^{-1} above the electronic origin, well into the S_2 electronically excited state.[28] Matrix isolation spectroscopy of the cation in argon matrix[34] and in solid H_2O[35] has been reported in the mid-IR and near-IR region from 600 to 1600 cm^{-1}. In this paper, we use resonantly enhanced multiphoton ionization (REMPI) to probe the vibronic structure of the first excited electronic state S_1, and the ZEKE technique to probe the skeletal modes of the cationic state D_0. Additional insights can be obtained from the results of ab initio and density functional calculations.

EXPERIMENTAL SETUP

The experimental apparatus is a differentially pumped molecular beam machine, with the detection chamber enclosed inside the source chamber.[21,23] A time-of-flight mass spectrometer in the detection chamber also serves as the pulsed field ionization zero kinetic energy photoelectron spectrometer. The sample B*ghi*P (Aldrich) had a specified purity of 98%, and altogether less than 100 mg was used throughout the whole experiment. It was housed and heated to 260 °C in a modified pulsed valve (General Valve, series 9) located in the source chamber to achieve sufficient vapor pressure. The vapor was seeded in 470 Torr of argon and coexpanded into a vacuum through a pulsed valve with a 1 mm orifice. After passing through a 2 mm skimmer, the cooled sample reached the detection chamber for laser excitation and ionization. The laser systems for the REMPI experiment included two Nd:YAG (Spectra Physics, GCR 190 and GCR 230) pumped dye lasers (Laser Analytical System, LDL 20505 and LDL 2051). The pump laser in the 397−372 nm range, obtained from the dye laser system (exalite 389, 384 and 376), had a pulsed energy of >1.0 mJ/pulse with a bandwidth of 0.5 cm^{-1}. The ionization laser in the 300−309 nm range from the

Table 1. Assignment of Vibrational Transitions (cm^{-1}) of the S_1 State of B*ghi*P[a,b]

REMPI	calc.[c]	assign.		droplet	calc.	assign.	abs.	calc.	assign.
449	443	$3a_1$	31^1	450.3					
472	471	$4a_1$	30^1	471.4	461.8	$4a_1$			
518	***521***	***$3b_1$***	79^1	517.3	504.9	$3b_1$	517.5	509.1	$3b_1$
553	***559***	***$4b_1$***	78^1	552.6	533.7	$4b_1$	552.7	533.2	$4b_1$
				611.2	603.4	$5b_1$			
675	670	$6b_1$	76^1	676.1	664.7	$6b_1$			
748	749	$7a_1$	27^1						
750	***769***	***$7b_1$***	75^1	752.5	759.5	$7b_1$	749.7	749.9	$7b_1$
757	773	$8b_1$	74^1	760.1			757.1	789.3	$8b_1$
				779.8	777.2	$1a_13b_1$			
				903.6	905.1	$9b_1$			
938	***935***	***$9b_1$***	73^1	936.6	950.1	$3a_13b_1$	937.1	908.2	$9b_1$
979	966	$9a_1$	25^1	978.4	978.9	$3a_14b_1$			
1002	***1002***	***$3a_14b_1$***	31^178^1	1001.1	995.5	$4a_14b_1$			
1014	***1012***	***$10b_1$***	72^1	1013.1	1025.2	$10b_1$	1012.8	1010.6	$10b_1$
1074	***1072***	***$11b_1$***	71^1	1073.1	1077.6	$11b_1$	1072	1067	$11b_1$
1080	***1081***	***$5a_14b_1$***	29^178^1	1075					
1132	1131	$12b_1$	70^1	1132		$1a_13b_1$	1131.7	1117	$13b_1$
1193	1193	$14b_1$	68^1	1194		$3a_17b_1$			
1196				1196.3					
1206				1207.5			1205.1	1204	$16b_1$

[a]Results from helium droplet are based on ref 28 and results from absorption (abs.) are from ref 29. [b]The bands that have yielded ZEKE spectra are in bold and italicized typeset. [c]The calculation was performed using TDDFT (root = 2) with a 6-31G basis set. The listed values include a scaling factor of 0.9549.

dx.doi.org/10.1021/jp2109576 | J. Phys. Chem. A 2012, 116, 1551−1557

frequency-doubled output of the other dye laser (rhodamine 610 and sulforhodamine 640 mix) had a pulse energy of ~1 mJ/pulse with a bandwidth of 0.3 cm^{-1}. The absolute wavelength of each laser was calibrated using an iron hollow-cathode lamp filled with neon. The pump laser and ionization laser were set to counter-propagate, and the light path, the flight tube, and the molecular beam were mutually perpendicular. The relative timing between the two laser pulses was controlled by two delay generators (Stanford Research, DG 535), and the optimal signal was obtained under temporal overlap between the pump and ionization lasers. In the ZEKE experiment, molecules excited to high Rydberg states were allowed to stay for 600 ns in the presence of a constant DC spoiling field of ~160 mV/cm, after which ionization and extraction were achieved by a pulsed electric field of ~2 V/cm.

Gaussian 09W suite[36] was used to optimize the molecular structure, to obtain vibrational frequencies, and to simulate the observed vibronic structures from REMPI and ZEKE. For the ground state of the neutral and the cationic state, density functional theory (DFT) calculations using the B3LYP functional were performed with the 6-31G (d,p) basis set. The excited state S_1 was calculated using both time-dependent density functional theory (TDDFT) with the B3LYP functional and the 6-31G basis set and the configuration interaction singles (CIS) with the 6-311G basis set. Details of the calculations will be provided in the following.

RESULTS

Two-Color 1 + 1′ REMPI Spectroscopy. The two-color 1 + 1′ REMPI spectrum of B*ghi*P near the origin of the $S_1 \leftarrow S_0$ electronic transition is displayed in Figure 1. The ionization laser was set at 33 280 cm^{-1} and was temporally and spatially overlapped with the scanning resonant laser. Each data point was an average of 100 laser shots, and the spectrum was repeatable over a 2-year period. The peak at 25 027 ± 3 cm^{-1} is assigned as the origin band, which agrees with the absorption study value of 25 027.1 ± 0.2 cm^{-1} by Rouillé et al.[29] Other observed vibronic transitions are listed in Table 1. Two labeling schemes are used in the table for comparison: one is to follow previous reports by numbering each symmetry species independently from low to high frequencies,[28,29] and the other is to follow the order of the symmetry species in the character table, and for a given species, in descending order of the frequency. Different definitions of the molecular axes result in different symmetry species for both the electronic state and the vibrational modes, and for clarity, the molecular axes of this work is also shown in the inset of Figure 1.

The two closely spaced electronically excited states of B*ghi*P imply potential confusions from TDDFT and CIS calculations. We calculated both electronic states using both methods. To our satisfaction, the results from both TDDFT and CIS are similar in terms of electronic configurations of the excited states and in vibrational frequencies. The putative S_1 state from the Gaussian program corresponds to an electronic transition from the highest occupied molecular orbital (HOMO) to the lowest unoccupied molecular orbital (LUMO) with a transition dipole perpendicular to the $C_2(z)$ symmetry axis and an oscillator strength of ~0.3. The putative S_2 state corresponds to electronic excitations of LUMO ← HOMO−1 and LUMO+1 ← HOMO, with $^1A_1$ symmetry and an oscillator strength of 0.002. We then further calculated the REMPI excitation spectra using the new vibronic coupling feature of Gaussian 09, and the resulting spectra from TDDFT calculations are shown in Figure 2. The transition to the $^1B_1$ state has a strong origin band and relatively weak vibronic activities, while the transition to the $^1A_1$ state qualitatively agrees with the experimental observation. We therefore believe that the observed transition correspond to the $^1A_1$ state, i.e., the putative S_2 state. On the other hand, no experimental evidence of lower lying electronic states was observed either in the solution or in the vapor phase from ultraviolet−visible (UV/vis) spectrometers. Since the S_1 state has a much higher oscillator strength and is within 2000 cm^{-1} of the origin of the S_2 state, we then concluded that the order of states from Gaussian is switched, and hence we labeled the $^1A_1$ state to be S_1, in agreement with previous literature reports.[28,29,37]

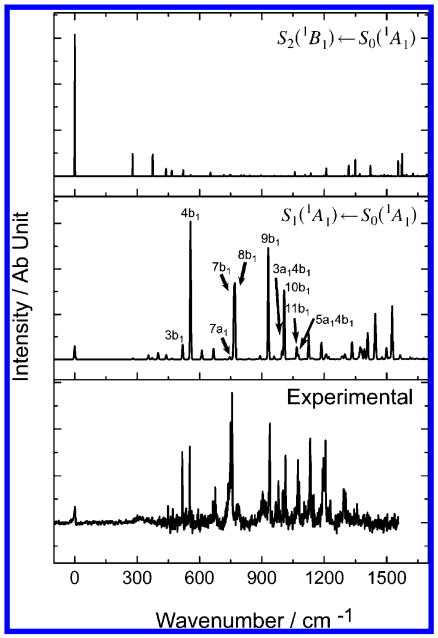

Figure 2. Excitation spectra calculated from Gaussian 09 for the two different electronic states. The experimental spectrum from Figure 1 is reproduced for comparison.

The agreement in Figure 2 greatly simplifies the vibrational assignment of the REMPI spectrum. All the observed vibrational modes can be assigned as either a_1 or b_1 symmetry species. B*ghi*P has 33 a_1 modes allowed by the FC principle in the $^1A_1 \leftarrow {}^1A_1$ transition, and among the 11 a_1 modes in the current spectral region, only five can be identified either as independent vibrational bands or in combination bands. Herzberg−Teller vibronic coupling with the $^1B_1$ state activates the FC forbidden but vibronically allowed b_1 modes. Interestingly, for B*ghi*P, the frequency distributions of a_1 and b_1 modes are similar, and within the current spectral range, a few more b_1 modes than a_1 modes can be identified. In addition, the intensities of the b_1 modes seem to be higher than those of the a_1 modes in Figure 1. The a_2 and b_2 modes are mostly out-of-plane bending motions that are only allowed for transitions to even quantum states, and they are not observable in the current spectrum.

Our assignment is in general agreement with previous literature reports.[28,29] The scaling factors, however, seem to vary substantially depending on the calculation method. The two different calculation methods from our own Gaussian 09 also resulted in very different scaling factors: 0.9549 for TDDFT 6-31G and 0.9049 for CIS 6-311G. Nevertheless, the

dx.doi.org/10.1021/jp2109576 | J. Phys. Chem. A 2012, 116, 1551−1557

qualities of both linear regressions are similarly high, with only the $7a_1$ and $10b_1$ modes that have discrepancies larger than 6 cm^{-1} for CIS (not listed in Table 1), and $7b_1$, $8b_1$, and $9a_1$ modes for TDDFT (Table 1).

ZEKE Spectroscopy. By scanning the ionization laser while setting the resonant laser at one of the intermediate states identified in the above REMPI experiment, we obtained pulsed field ionization ZEKE spectra as shown in Figures 3 and 4. The

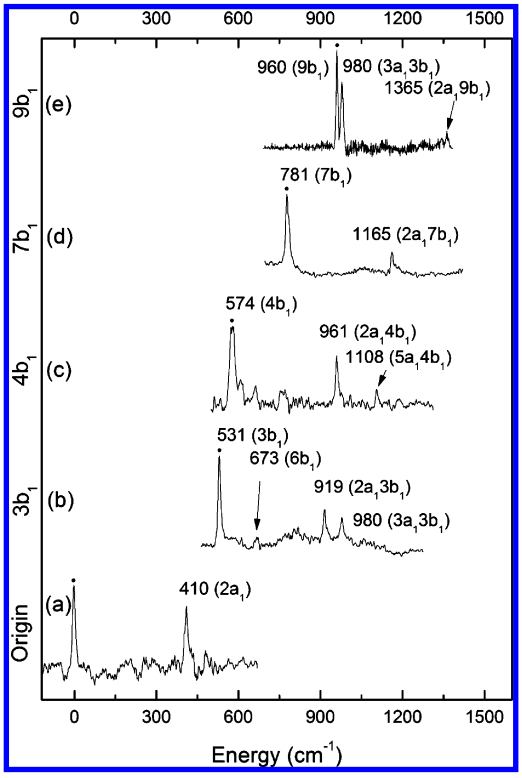

Figure 3. Two-color ZEKE spectra of B*ghi*P recorded via five of the vibrational levels of the S_1 state as intermediate states. The energy in the *x*-axis is relative to the ionization threshold at 57 623 cm^{-1}. The labels in the figure refer to the vibrational energies in cm^{-1} and symmetry assignments of the cation, and the corresponding vibrational assignment of the intermediate state is labeled by a black dot in each panel. The assignment can be found in Table 2.

reproducibility of the spectra was tested over a 2-year period. The spectra in Figure 3 were obtained with about 100 laser shots per data point, but the spectra in Figure 4 were recorded with more than 200 laser shots per data point due to the low signal intensity. The two figures are plotted on different horizontal scales for clarity and compactness. The identity of the vibrational level of the intermediate state for each ZEKE spectrum is labeled in the corresponding panel by a black dot. The experimental and theoretical values are shown in Table 2. The calculation for the cation vibrational frequencies was performed at the B3LYP/6-31G (d,p) level. Using a least-squares fitting procedure similar to that for the S_1 state, we obtained a scaling factor of 0.9983 with a coefficient of determination 0.9995. Limited by the line width of the resonant transitions and the pulsed electric field, the uncertainty of the experimental values of the ZEKE spectra is ±7 cm^{-1}.

Trace 3a was recorded via the origin of the S_1 state, and the most intense peak corresponds to the origin of the cation. The adiabatic ionization potential is thus determined to be 57 623 ± 7 cm^{-1} (7.1443 ± 0.0006 eV). This value is about 300 cm^{-1}

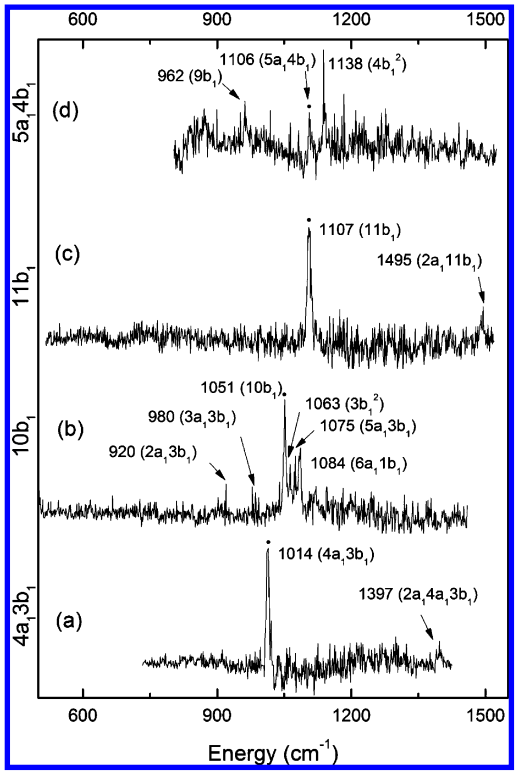

Figure 4. The two-color ZEKE spectra of B*ghi*P recorded via four of the vibrational levels of the S_1 state as intermediate states. The energy in the *x*-axis is relative to the ionization threshold at 57 623 cm^{-1}. The labels in the figure refer to the vibrational energies in cm^{-1} and symmetry assignments of the cation, and the corresponding vibrational assignment of the intermediate state is labeled by a black dot in each panel. The assignment can be found in Table 2.

lower than that of 7.19 ± 0.01 eV from photoelectron spectroscopy by Boschi, Murrell, and Schmidt in 1972[38] and close to the result of 7.15 eV from gas phase ion equilibrium measurements by Meot-Ner in 1980.[39] Our new value represents an improvement of 1 order of magnitude in precision for the ionization threshold.

In addition to the origin band, trace 3a also contains a $2a_1$ band of the cation, in agreement with the symmetry selection rule dictated by the FC factor. Using Gaussian 09 and based on the geometry and vibrational information of the intermediate (TDDFT 6-31G) and the cationic state (DFT B3LYP/6-31G (d,p)), we were able to calculate the ionization spectrum from the origin band and the comparison is shown in Figure 5. The excellent agreement between calculation and experiment further confirms the assignment of the $2a_1$ mode for the cation, although the frequency difference between experiment and calculation, even after a scaling factor of 0.9983, is still on the order of 20 cm^{-1}.

Except for trace 3a, the rest of the ZEKE spectra were obtained from b_1 intermediate vibronic states and almost all observed vibrational bands in the ZEKE spectra are of b_1 symmetry. Most vibronic transitions in the REMPI spectrum of Figure 1 that are of b_1 symmetry with a signal-to-noise ratio above 5 were successful candidates as intermediate states for ZEKE experiments. The only exception is the $8b_1$ band, which is in close proximity to the $7b_1$ band and is of similar intensity, but no ZEKE signal was observable from this band.

The ZEKE spectra in Figures 3 and 4 are sparse, and the most salient feature is the dominance of the same vibrational

dx.doi.org/10.1021/jp2109576 | J. Phys. Chem. A 2012, 116, 1551−1557

Table 2. Vibrational Assignment of B*ghi*P cation relative to the 57623 cm^{-1} ionization threshold[a]

0°	$3b_1$	$4b_1$	$7b_1$	$9b_1$	$4a_13b_1$	$10b_1$	$11b_1$	$5a_14b_1$	calc[b]	assignment	
410									390	$2a_1$	32^+
	531								531	$3b_1$	79^+
		574							567	$4b_1$	78^+
	673								686	$6b_1$	76^+
			781						783	$7b_1$	75^+
	919					920			921	$2a_13b_1$	32^+79^+
				960				962	949	$9b_1$	73^+
		961							957	$2a_14b_1$	32^+78^+
	980			980		980			988	$3a_13b_1$	31^+79^+
					1014			1019	1024	$4a_13b_1$	30^+79^+
						1051			1054	$10b_1$	72^+
						1063			1062	$3b_1^2$	79^{2+}
						1075			1073	$5a_13b_1$	29^+79^+
						1084			1082	$6a_11b_1$	28^+81^+
							1107		1115	$11b_1$	71^+
		1108						**1106**	1109	$5a_14b_1$	29^+78^+
								1138	1134	$4b_1^2$	78^{2+}
			1165						1173	$2a_17b_1$	32^+75^+
				1365					1348	$2a_19b_1$	32^+73^+
					1397				1415	$2a_14a_13b_1$	$32^+30^+79^+$
							1495		1505	$2a_111b_1$	32^+71^+

[a]Transitions in bold typeface are of the same symmetry as that of the intermediate state. [b]The calculation result includes a scaling factor of 0.9983.

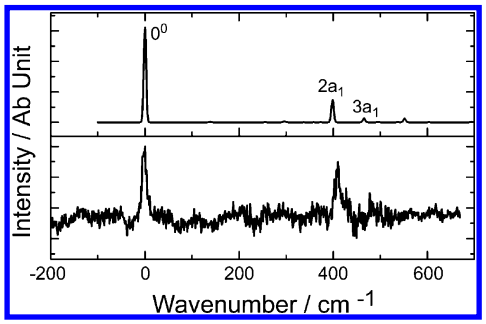

Figure 5. FC calculation using Gaussian 09 from the origin of the S_1 state to the D_0 state. The experimental spectrum from trace 3a is reproduced for comparison.

level as that of the S_1 intermediate state, with the exception of trace 4d. This propensity in preserving the vibrational excitation of the intermediate state can also offer further guidance in assignment of both the REMPI and ZEKE spectra, particularly for high energy bands where more than one potential candidate of combination bands might exist. For example, the peak at 961 cm^{-1} in trace 3c and the peak at 960 cm^{-1} in trace 3e are assigned as two different transitions, despite of the fact that our experimental uncertainty is 7 cm^{-1}. Trace 3c was recorded from the $4b_1$ intermediate state, hence it would be more reasonable to assign the transition at 961 cm^{-1} as a combination band with mode $4b_1$ than to assign it as a completely different vibrational mode. On the other hand, trace 3e was recorded via the $9b_1$ level of the S_1 state, and its dominant transition should correspond to the same vibrational mode of the cation. Given the fact that the calculated frequencies for both vibrational levels of the cation are virtually degenerate, we thus believe that the two peaks from the two different spectra should have two different identities. A similar argument holds for the transitions between 1106 and 1108 cm^{-1} in traces 3c, 4c, and 4d.

Another noticeable feature of the ZEKE spectra is the repetition of the vibrational pattern of trace 3a: most ZEKE traces contain a dominant band and a combination band with mode $2a_1$, similar to the ZEKE spectrum from the electronic origin of the S_1 state. This consistency further offers confirmation of the vibrational assignment. More importantly, the qualitative agreement between the FC calculation in Figure 5 and trace 3a implies that although vibronic coupling is extensive for the intermediate state, the ionization process is largely unperturbed, and the FC principle is more or less preserved.

The two ZEKE spectra that do not exhibit the same pattern as trace 3a are traces 4b and 4d. The overall intensities of these two spectra are also substantially lower than those from Figure 3. The quartet feature of trace 4b poses a challenge for a definitive assignment. On the basis of the frequent appearance of mode $3b_1$ at 920 and 980 cm^{-1}, two of the four peaks can be assigned as combination bands with mode $3b_1$. The triplet feature at 980 cm^{-1} is also present in traces 3b and 3e, although because of the compact horizontal scale, the splitting is not discernible in Figure 3. We could only attribute the lowest energy component of the triplet to a combination band of mode $3b_1$.

DISCUSSION

S_1 State. The new capability of Gaussian 09 to include vibronic coupling for calculations of excitation spectroscopy is truly remarkable. The agreement between simulation and experiment for both the REMPI and ZEKE spectra helps greatly with the vibrational assignment and determination of symmetry and electronic orbitals of the related states. Discussions on the symmetry and nature of the first two electronically excited states of B*ghi*P have had a long history. On the basis of experiments both in the gas phase and in the solution phase and on advanced theoretical calculations, the S_1 state is generally considered $^1A_1$, and the S_2 state is considered $^1B_1$.[29,31,33,40−42] Our work confirms the previous conclusion based on simulations of the excitation spectra. However, even with Gaussian 09, the order of the electronic excitation is still

dx.doi.org/10.1021/jp2109576 | J. Phys. Chem. A 2012, 116, 1551−1557

switched. To obtain the current calculation result, the keyword for the Gaussian input has to be set to root = 2.

The vibrational distribution of B*ghi*P should be compared with those of pyrene[21] and benzo[a]pyrene (B*a*P),[43] two other peri-condensed PAHs that have been investigated in our group, and those of a few cata-condensed PAHs.[22,23,44,45] In the REMPI spectrum of pyrene,[21] two types of vibrational bands were observed, and the FC-allowed in-plane stretching modes were relatively stronger than the out-of-plane vibronic modes. The addition of another ring off the symmetry axis of pyrene in B*a*P lowered the symmetry point group to C_s.[43] Although configuration interaction remained, the two interacting electronic states in B*a*P were of the same symmetry and the resulting FC profiles were similar. Consequently, a FC calculation from our TDDFT results had qualitatively reproduced the observed spectrum. As the molecular frame expanded symmetrically from pyrene to B*ghi*P, the symmetry point group lowered to C_{2v}, and vibronic modes overtook the FC modes, dominating the REMPI spectrum. In contrast, cata-condensed PAHs including tetracene and pentacene were not affected by configuration interactions.[22,23] The REMPI spectrum of tetracene was dominated by FC bands,[23] although FC simulations without vibronic coupling resulted in an overly strong origin band. Pentacene was sufficiently flexible in the molecular frame,[22] and the out-of-plane waving modes of the ribbon dominated the REMPI spectrum. Within this selected group of PAHs, we therefore conclude that both symmetry and size affect the vibrational distribution upon electronic excitation. Lower symmetry systems exhibit more FC behavior, and expansion of the molecular frame exacerbates non-FC behaviors.

D_0 State. In contrast to the strong vibronic activities of the REMPI spectrum, the ZEKE spectra of B*ghi*P exhibit strong FC behavior. The pattern for the vibrational distribution of the origin band is repeated in most of the observed ZEKE spectra originating from different intermediate vibrational states. This situation is also an indicator of the capacity of the molecular frame for accommodating the additional charge upon ionization. Among the PAHs that we have investigated,[21−23,43] only B*a*P has demonstrated a propensity of preserving the vibrational excitation of the intermediate state,[43] which agrees with the high structural stability of the low symmetry PAHs. No obvious propensity has been observed in pyrene, tetracene, and pentacene.[21−23]

On the basis of our previous studies of cata-condensed PAHs and a series of small benzene derivatives,[21−23,46−50] DFT calculations typically yield reliable vibrational frequency information for the cation. In the case of B*ghi*P, a scaling factor of 0.9983 is needed to fit the experimental frequencies, and mode $2a_1$ is proven an outlier with a deviation much larger than the experimental uncertainty. This agreement is on par with the case of B*a*P[43] but worse than the cases of pyrene, tetracene, and pentacene where no scaling factor was needed.[21−23] This variation of scaling factors is unsettling, particularly for predictions of vibrational bands from unknown substances.

All observed modes including b_1 and a_1 modes in ZEKE are IR active; however, a direct frequency comparison with results from literature reports is still impossible. Hudgins and Allamandola reported the cation IR spectroscopy of B*ghi*P in argon matrices from 600 cm^{-1} to 1600 cm^{-1}.[51] Bernstein et al. studied the cation IR spectroscopy in solid water from 1120 cm^{-1} to 1600 cm^{-1}.[35] Within the range of frequency overlap with our current work, unfortunately, these two studies failed to observe any b_1 or a_1 modes, perhaps due to the low transition intensities of these modes. This situation alludes to the value of ZEKE spectroscopy for astrophysical studies: although the vibrational intensities from ZEKE are not representative of single photon absorption or emission, the frequency information is still valuable for calibration and for optimization of scaling factors from calculation. Furthermore, for noncentral symmetric PAHs such as B*ghi*P, vibrational frequencies from ZEKE can be used for direct line identification.

CONCLUSION

Vibrational properties of the electronically excited and ionic states of B*ghi*P have been studied using REMPI and ZEKE. Due to strong Herzberg−Teller coupling, vibronic allowed bands of the first excited state dominate the REMPI spectrum, much stronger in intensity than those of FC allowed a_1 modes. With the vibronic coupling feature of Gaussian 09, on the other hand, the REMPI spectrum can be simulated with remarkable success. The ZEKE spectra demonstrate a propensity for preserving the vibrational excitation of the intermediate state. The vibrational pattern of the ZEKE spectrum from the origin of the S_1 state can be reproduced by a direct FC calculation, and the vibrational pattern is more or less repeated for most ZEKE spectra originating from intermediate vibronic b_1 states. These observations confirm the invariance of the molecular frame upon ionization. All observed modes in ZEKE are IR active, but none of the observed modes have ever been reported from previous IR experiments. This result establishes the role of ZEKE in mapping out the vibrational mode distribution of PAHs for astrophysical studies.

AUTHOR INFORMATION

Corresponding Author

*E-mail: wei.kong@oregonstate.edu; fax: 541-737-2062.

ACKNOWLEDGMENTS

This work is supported by the National Aeronautics and Space Administration under award No. NNX09AC03G.

REFERENCES

(1) Tielens, A. G. G. M. *Annu. Rev. Astron. Astrophys.* **2008**, *46*, 289−337.

(2) Smith, L. E.; Denissenko, M. F.; Bennett, W. P.; Li, H.; Amin, S.; Tang, M.-S.; Pfeifer, G. P. *J. Natl. Cancer Inst.* **2000**, *92*, 803−811.

(3) Harvey, R. G. *Polycyclic Aromatic Hydrocarbons: Chemistry and Carcinogenicity*; Cambridge University Press: London, 1991.

(4) Mulas, G.; Malloci, G.; Joblin, C.; Toublanc, D. *Astron. Astrophys.* **2006**, *456*, 161−169.

(5) Bernstein, M. P.; Dworkin, J. P.; Sandford, S. A.; Cooper, G. W.; Allamandola, L. J. *Nature* **2002**, *416*, 401−403.

(6) Shock, E. L.; Schulte, M. D. *Nature* **1990**, *343*, 728−731.

(7) Wakeham, S. G.; Schaffner, C.; Giger, W. *Geochim. Cosmochim. Acta* **1980**, *44*, 415−429.

(8) Li, A. PAHs in Comets: An Overview. In *Deep Impact as a World Observatory Event: Synergies in Space, Time, and Wavelength*; Kaufl, H. U., Siebenmorgen, R., Moorwood, A. F. M., Eds.; Springer: Berlin, 2009; pp 161−175.

(9) Peeters, E.; Allamandola, L. J.; Hudgins, D. M.; Hony, S.; Tielens, A. G. G. M. *Astron. Soc. Pac. Conf. Ser.* **2004**, *309*, 141−162.

(10) Malloci, G.; Mulas, G.; Benvenuti, P. *Astron. Astrophys.* **2003**, *410*, 623−637.

(11) Mulas, G.; Malloci, G.; Benvenuti, P. *Astron. Astrophys.* **2003**, *410*, 639−648.

(12) Langhoff, S. R. *J. Phys. Chem.* **1996**, *100*, 2819−2841.
(13) Parisel, O.; Berthier, G.; Ellinger, Y. *Astron. Astrophys.* **1992**, *266*, L1−L4.
(14) Allamandola, L. J.; Tielens, A. G. G. M.; Barker, J. R. *Astrophys. J.* **1985**, *290*, L25−L28.
(15) Léger, A.; Puget, J., L. *Astron. Astrophys.* **1984**, *137*, L5−L8.
(16) Qi, F.; Yang, R.; Yang, B.; Huang, C.; Wei, L.; Wang, J.; Sheng, L.; Zhang, Y. *Rev. Sci. Instrum.* **2006**, *77*, 084101.
(17) Biennier, L.; Salama, F.; Gupta, M.; O'keefe, A. *Chem. Phys. Lett.* **2004**, *387*, 287−294.
(18) Hudgins, D. M. *Polycyclic Aromat. Compd.* **2002**, *22*, 469−488.
(19) Joblin, C.; Berné, O.; Simon, A.; Mulas, G. *arXiv:0904.3185*, 2009
(20) Zhang, K.; Guo, B.; Colarusso, P.; Bernath, P. F. *Science* **1996**, *274*, 582−583.
(21) Zhang, J.; Han, F.; Kong, W. *J. Phys. Chem. A* **2010**, *114*, 11117−11124.
(22) Zhang, J.; Han, F.; Li, A.; Kong, W. *Astrophy. J.* **2010**, *715*, 485−492.
(23) Zhang, J.; Pei, L.; Kong, W. *J. Chem. Phys.* **2008**, *128*, 104301.
(24) Merkt, F.; Schmutz, H. *J. Chem. Phys.* **1998**, *108*, 10033−10045.
(25) Li, A.; Luning, J. I. *Astrophy. J.* **2003**, *594*, 987−1010.
(26) Li, A.; Draine, B. T. *Astrophy. J.* **2002**, *576*, 762−772.
(27) Li, A.; Draine, B. T. *Astrophy. J.* **2001**, *554*, 778−802.
(28) Birer, Ö.; Moreschini, P.; Lehmann, K. K. *Phys. Chem. Chem. Phys.* **2008**, *10*, 1648−1657.
(29) Rouillé, G.; Arold, M.; Staicu, A.; Krasnokutski, S.; Huisken, F.; Henning, T.; Tan, X.; Salama, F. *J. Chem. Phys.* **2007**, *126*, 174311.
(30) Tan, X.; Salama, F. *J. Chem. Phys.* **2005**, *123*, 014312.
(31) Chillier, X.; Boulet, P.; Chermette, H.; Salama, F.; Weber, J. *J. Chem. Phys.* **2001**, *115*, 1769−1776.
(32) Birks, J. B.; Easterly, C. E.; Christophorou, L. G. *J. Chem. Phys.* **1977**, *66*, 4231−4236.
(33) Aihara, J.-i.; Ohno, K.; Inokuchi, H. *Bull. Chem. Soc. Jpn.* **1970**, *43*, 2435−2439.
(34) Hudgins, D. M.; Sandford, S. *J. Phys. Chem. A* **1998**, *102*, 344−352.
(35) Bernstein, M. P.; Sandford, S. A.; Mattioda, A. L.; Allamandola, L. J. *Astrophys. J.* **2007**, *664*, 1264−1272.
(36) Frisch, M. J. et al. *Gaussian 09*, revision B.01, Gaussian, Inc.: Wallingford, CT, 2004.
(37) Nijegorodov, N.; Mabbs, R.; Downey, W. S. *Spectrochim. Acta, Part A* **2001**, *57*, 2673−2685.
(38) Boschi, R.; Murrell, J. N.; Schmidt, W. *Faraday Discuss. Chem. Soc.* **1972**, *54*, 116−126.
(39) Meot-Ner, M. *J. Chem. Phys.* **1980**, *84*, 2716−2723.
(40) Dierksen, M.; Grimme, S. *J. Chem. Phys.* **2004**, *120*, 3544−3554.
(41) Palewska, K.; Chojnacki, H. *J. Mol. Struct.* **2002**, *611*, 23−32.
(42) Hummel, R. L.; Redenberg, K. *J. Chem. Phys.* **1962**, *66*, 2334−2359.
(43) Zhang, J.; Harthcock, C.; Fangyuan, H.; Kong, W. *J. Chem. Phys.* **2011**, *135*, 244306.
(44) Piuzzi, F.; Dimicoli, I.; Mons, M.; Millié, P.; Brenner, V.; Zhao, Q.; Soep, B.; Tramer, A. *Chem. Phys.* **2002**, *275*, 123−147.
(45) Syage, J. A.; Wessel, J. E. *J. Chem. Phys.* **1988**, *89*, 5962−5963.
(46) He, Y.; Kong, W. *J. Chem. Phys.* **2006**, *124*, 2043061.
(47) He, Y.; Wu, C.; Kong, W. *J. Chem. Phys.* **2004**, *121*, 8321−8328.
(48) He, Y.; Wu, C.; Kong, W. *Chem. Phys. Lett.* **2004**, *391*, 38−43.
(49) He, Y.; Wu, C.; Kong, W. *J. Chem. Phys.* **2004**, *121*, 3533−3539.
(50) Wu, C.; He, Y.; Kong, W. *Chem. Phys. Lett.* **2004**, *398*, 351−356.
(51) Hudgins, D. M.; Allamandola, L. J. *J. Phys. Chem.* **1995**, *99*, 3033−3046.